Aalborg Universitet

AALBORG UNIVERSITY

Large-Signal Modeling of Virtual Admittance-Based Grid-Forming Inverter

Huang, Liang; Blaabjerg, Frede; Chaudhary, Sanjay K.; Cui, Boyuan; Gao, Guoqing; Zhou, Dao

Published in:
2025 Energy Conversion Congress & Expo Europe (ECCE Europe)

DOI (link to publication from Publisher):
10.1109/ECCE-Europe62795.2025.11238623

Publication date:
2025

Document Version
Accepted author manuscript, peer reviewed version

Link to publication from Aalborg University

Citation for published version (APA):
Huang, L., Blaabjerg, F., Chaudhary, S. K., Cui, B., Gao, G., & Zhou, D. (2025). Large-Signal Modeling of Virtual Admittance-Based Grid-Forming Inverter. In *2025 Energy Conversion Congress & Expo Europe (ECCE Europe)* (pp. 1-6). IEEE (Institute of Electrical and Electronics Engineers). https://doi.org/10.1109/ECCE-Europe62795.2025.11238623

General rights
Copyright and moral rights for the publications made accessible in the public portal are retained by the authors and/or other copyright owners and it is a condition of accessing publications that users recognise and abide by the legal requirements associated with these rights.

- Users may download and print one copy of any publication from the public portal for the purpose of private study or research.
- You may not further distribute the material or use it for any profit-making activity or commercial gain
- You may freely distribute the URL identifying the publication in the public portal -

Take down policy
If you believe that this document breaches copyright please contact us at vbn@aub.aau.dk providing details, and we will remove access to the work immediately and investigate your claim.

Downloaded from vbn.aau.dk on: May 23, 2026

© 2025 IEEE. Personal use of this material is permitted. Permission from IEEE must be obtained for all other uses, in any current or future media, including reprinting/republishing this material for advertising or promotional purposes, creating new collective works, for resale or redistribution to servers or lists, or reuse of any copyrighted component of this work in other works.

Large-Signal Modeling of Virtual Admittance-Based Grid-Forming Inverter

Liang Huang
AAU Energy
Aalborg University
Aalborg, Denmark
lihu@energy.aau.dk

Frede Blaabjerg
AAU Energy
Aalborg University
Aalborg, Denmark
fbl@energy.aau.dk

Sanjay Chaudhary
AAU Energy
Aalborg University
Aalborg, Denmark
skc@energy.aau.dk

Boyuan Cui
Dept. of Electronic Engineering
The Chinese Univ. of Hong Kong
Hong Kong, China
cuiboyuan@link.cuhk.edu.hk

Guoqing Gao
AAU Energy
Aalborg University
Aalborg, Denmark
gga@energy.aau.dk

Dao Zhou
AAU Energy
Aalborg University
Aalborg, Denmark
zda@energy.aau.dk

***Abstract*—As wind power capacities increase, the decreasing inertia of modern power systems challenges its frequency stability. Unlike traditional grid-following inverters, grid-forming (GFM) inverters can create and stabilize a grid independent of the utility. Hence, GFM inverters are seen as a potential solution, but their transient stability is a growing concern. While large-signal models are effective tools for analyzing transient stability, most existing research focuses on typical GFM control schemes without using virtual impedance. To address such a research gap, this paper proposes several simplified large-signal models for GFM inverters with virtual admittance, showing that the second-order model closely matches the accuracy of the full-order EMT model. So, the second-order large-signal model is a competing candidate for transient stability analysis due to its simplicity and accuracy. Finally, the correctness of the proposed models has been verified by time-domain simulations.**

Keywords—large-signal model, grid-forming inverter, virtual admittance, low voltage fault, transient stability.

I. INTRODUCTION

Grid-forming inverters have gained significant attention in recent years due to their pivotal role in enabling the integration of renewable energy sources into power grids [1], [2]. Unlike traditional grid-following inverters, which rely on an existing grid to synchronize, grid-forming (GFM) inverters can create and stabilize a grid independent of the utility [3], [4], [5]. This capability is crucial for supporting the transition toward a more sustainable energy system, particularly with increasing contributions from renewable energy sources like solar and wind power [6]. Although the GFM inverter technology is considered as a promising solution for the future power system, it still has some technical challenges to be addressed, such as transient stability issues during large grid disturbances [7], [8], [9].

To study the transient stability, large-signal models are effective tools for stability analysis [10]. However, due to the mathematical challenge of solving high-order nonlinear differential equations, model order reduction is necessary. Therefore, in most existing research, the GFM inverter is usually simplified to be a second-order large-signal model for stability analysis, which only includes the dynamics of the virtual inertia and the power angle [11], [12], [13], [14]. However, the existing research mainly focuses on the typical GFM control scheme with cascaded voltage and current controllers, while the large-signal model of the virtual admittance-based GFM inverter has not been studied thoroughly.

Therefore, this paper focuses on building large-signal models of the virtual admittance-based GFM inverters and the influence of relevant parameters on transient stability. To simplify the analysis, the current control loop of the GFM inverter is assumed to be an ideal controlled current source (CCS) initially. Thus, the influences of the current control loop dynamics and the other dynamics are able to be separated, which is beneficial for a simpler model representation. Then, an eighth-order large-signal model of the GFM inverter is built, which can represent the GFM CCS accurately. Afterward, the eighth-order large-signal model is simplified to be a fourth-order model by ignoring the filter capacitance and the dynamics of the grid inductors. Further, the fourth-order model is simplified as a second-order model by neglecting the dynamics of the virtual inductors. It is found that the accuracy of the second-order, the fourth-order, and the eighth-order large-signal models is almost as high as the EMT model of the virtual admittance-based GFM inverter. Therefore, the dynamics of the current control loop, filter capacitors, grid inductors, and virtual inductors are negligible for large-signal stability analysis.

The overall structure of the paper is organized as follows: Section II discusses the large-signal modeling process of GFM inverters, presenting several reduced-order models. Afterward, Section III provides mathematical expressions for these different reduced-order models. Subsequently, Section IV introduces several case studies to illustrate conditions that may lead to transient instability of GFM inverters. Finally, Section V concludes this paper.

This work is supported by the Offshore Energy Hubs research project.

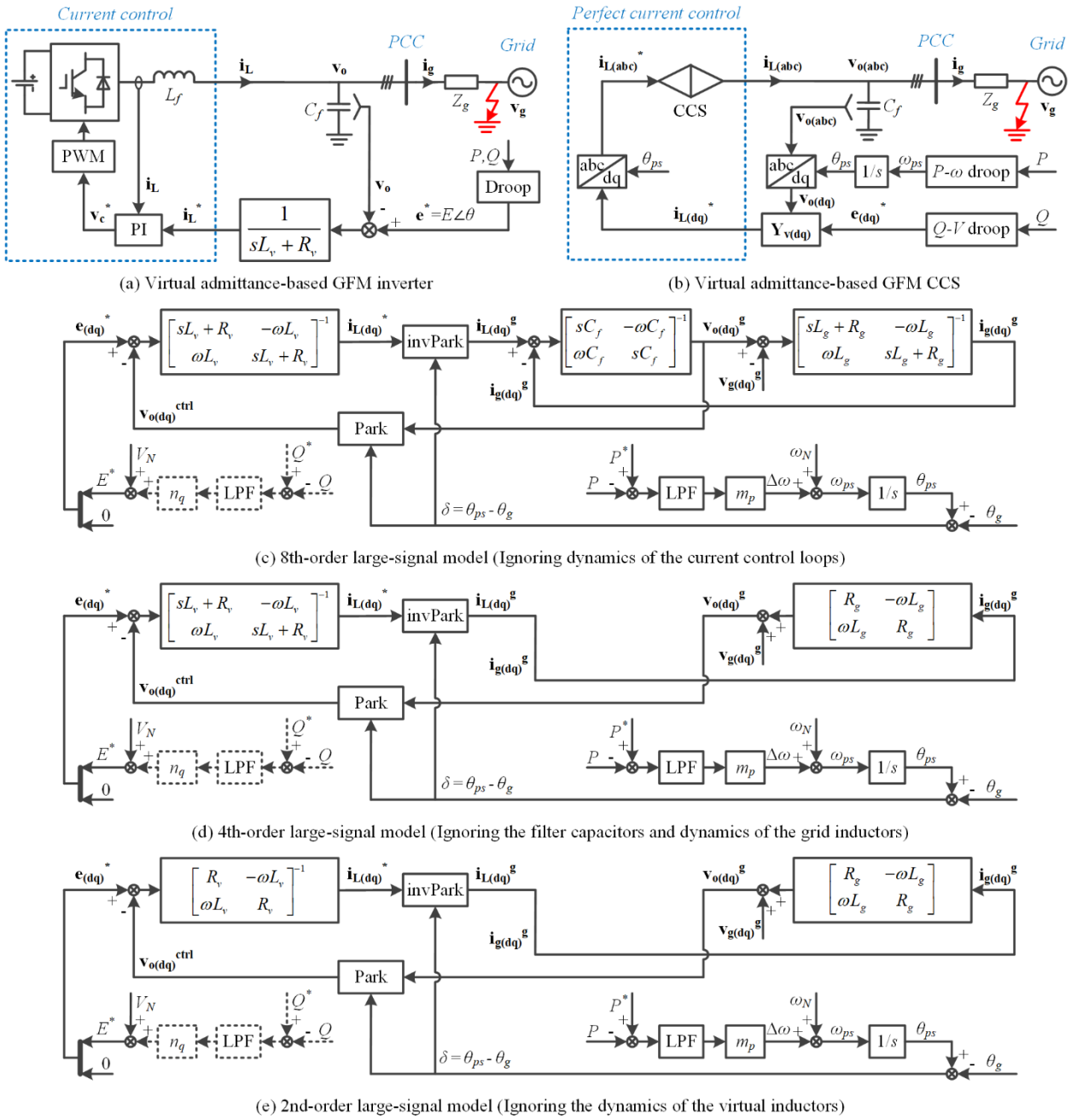

Fig. 1. Reduced-order large-signal models of virtual admittance-based grid-forming inverter.

II. Large-Signal Modeling of Grid-Forming Inverter

The physical configuration of the study system is shown in Fig. 1(a), which includes a GFM inverter and a Thevenin equivalent grid. The GFM inverter connects to the power grid at the point of common coupling (PCC). The typical virtual admittance-based GFM control scheme is chosen for analysis, which is the same as the control method presented in [4].

To simplify the analysis, the current control loop is replaced with an ideal CCS, shown in Fig. 1(b). Based on the GFM CCS, an 8th-order large-signal model in the d-q frame can be derived, as illustrated in Fig. 1(c). Notably, the *Q-V* droop is ignored as it is less important for synchronization. Besides, the superscript 'g' represents variables in the grid d-q frame, while the superscript 'ctrl' represents variables in the control d-q frame. Subsequently, by neglecting the filter capacitors and the dynamics of the grid inductors, the 8th-order large-signal model can be simplified as a 4th-order model, as depicted in Fig. 1(d). Additionally, by neglecting the dynamics of the virtual inductors, the 4th-order large-signal model can be simplified to a 2nd-order model, as presented in Fig. 1(e). Time-domain simulation results of these models are compared in Fig. 2.

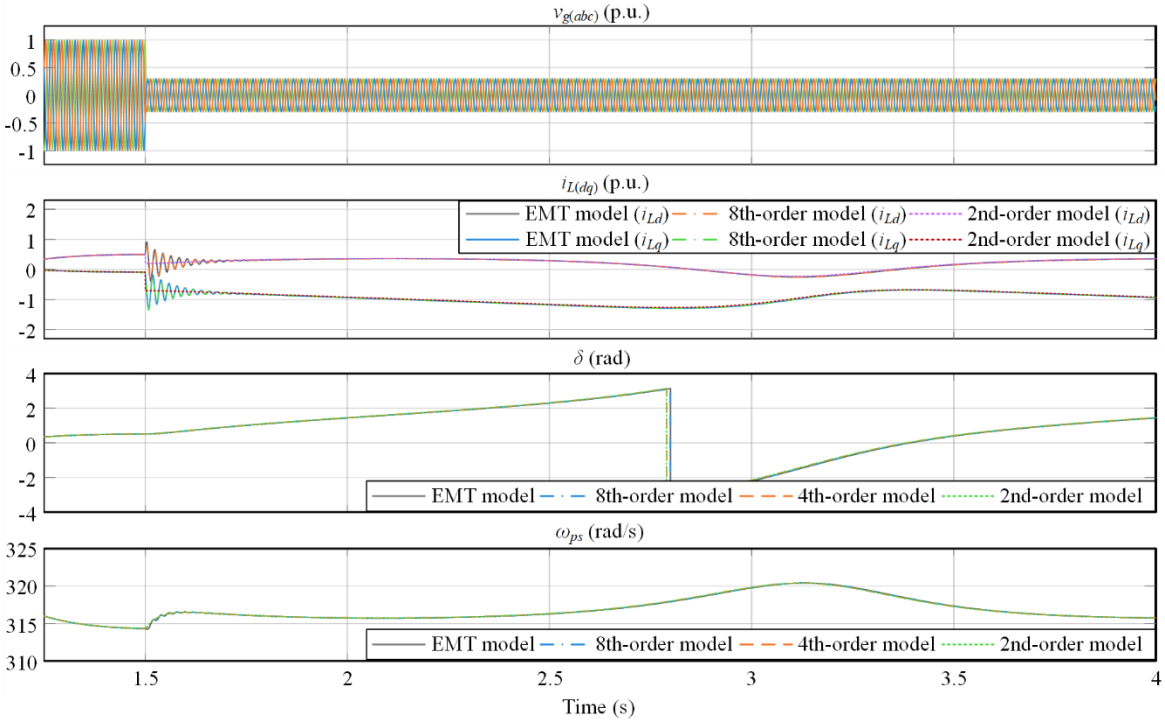

Fig. 2. Comparison of different models by time-domain simulation (Condition: P = 0.5 p.u., SCR = 2, V_g sags to 0.3 p.u.).

Fig. 2 shows that dynamic responses of the 8th-order model, the 4th-order model, and the 2nd-order model are highly similar to one another after grid voltage sags to 0.3 p.u. Thus, the 2nd-order model is a good candidate for the transient stability analysis of the GFM inverter, because it is simple and accurate.

III. Mathematical Expressions of Reduced-Order Large-Signal Models

The analysis in the previous section basically relies on simulations, which is time-consuming. A more efficient way is to use an Ordinary Differential Equation (ODE) solver to obtain the numerical solutions, which will be discussed in this section.

A. Eighth-Order Large-Signal Model

First of all, based on Fig. 1(c), the dynamics of the active power controller can be described by (1) and (2).

$$\dot{\delta} = \Delta\omega + \omega_N - \omega_g \tag{1}$$

$$\Delta\dot{\omega} = -\omega_{LPF} \cdot \Delta\omega + \omega_{LPF} \cdot m_p \cdot (P^* - P) \tag{2}$$

Moreover, the dynamics of the grid impedance and the filter capacitors can be represented by (3) and (4).

$$\begin{cases} L_g \dot{i}_{gd}^{\ g} + R_g i_{gd}^{\ g} - \omega_N L_g i_{gq}^{\ g} = v_{od}^{\ g} - v_{gd}^{\ g} \\ \omega_N L_g i_{gd}^{\ g} + L_g \dot{i}_{gq}^{\ g} + R_g i_{gq}^{\ g} = v_{oq}^{\ g} - v_{gq}^{\ g} \end{cases} \tag{3}$$

$$\begin{cases} C_f \dot{v}_{od}^{\ g} - \omega_N C_f v_{oq}^{\ g} = i_{Ld}^{\ g} - i_{gd}^{\ g} \\ \omega_N C_f v_{od}^{\ g} + C_f \dot{v}_{oq}^{\ g} = i_{Lq}^{\ g} - i_{gq}^{\ g} \end{cases} \tag{4}$$

In addition, the inverse Park transformation of the currents and the Park transformation of the PCC voltages are given by (5) and (6).

$$\begin{cases} i_{Ld}^{\ g} = \cos(\delta) \cdot i_{Ld}^{\ *} - \sin(\delta) \cdot i_{Lq}^{\ *} \\ i_{Lq}^{\ g} = \sin(\delta) \cdot i_{Ld}^{\ *} + \cos(\delta) \cdot i_{Lq}^{\ *} \end{cases} \tag{5}$$

$$\begin{cases} v_{od}^{\ \text{ctrl}} = \cos(\delta) \cdot v_{od}^{\ g} + \sin(\delta) \cdot v_{oq}^{\ g} \\ v_{oq}^{\ \text{ctrl}} = -\sin(\delta) \cdot v_{od}^{\ g} + \cos(\delta) \cdot v_{oq}^{\ g} \end{cases} \tag{6}$$

The virtual admittance is represented by (7).

$$\begin{cases} L_v \dot{i}_{Ld}^{\ *} + R_v i_{Ld}^{\ *} - \omega_N L_v i_{Lq}^{\ *} = e_d^{\ *} - v_{od}^{\ \text{ctrl}} \\ \omega_N L_v i_{Ld}^{\ *} + L_v \dot{i}_{Lq}^{\ *} + R_v i_{Lq}^{\ *} = e_q^{\ *} - v_{oq}^{\ \text{ctrl}} \end{cases} \tag{7}$$

Therefore, the 8th-order large-signal model can be obtained by combining (1)-(7), where the state variables are [δ, $\Delta\omega$, $v_{od}^{\ g}$, $v_{oq}^{\ g}$, $i_{gd}^{\ g}$, $i_{gq}^{\ g}$, $i_{Ld}^{\ *}$, $i_{Lq}^{\ *}$].

B. Fourth-Order Large-Signal Model

As presented in Fig. 1(d), when the filter capacitors are ignored, (4) can be simplified as (8).

$$\begin{cases} i_{Ld}^{\ g} = i_{gd}^{\ g} \\ i_{Lq}^{\ g} = i_{gq}^{\ g} \end{cases} \tag{8}$$

Besides, when the dynamics of the grid inductors are neglected, (3) can be simplified as (9).

$$\begin{cases} R_g i_{gd}{}^{g} - \omega_N L_g i_{gq}{}^{g} = v_{od}{}^{g} - v_{gd}{}^{g} \\ \omega_N L_g i_{gd}{}^{g} + R_g i_{gq}{}^{g} = v_{oq}{}^{g} - v_{gq}{}^{g} \end{cases} \quad (9)$$

Hence, the 4th-order large-signal model is able to be obtained by combining (1), (2), and (5)-(9), where the state variables are $[\delta, \Delta\omega, i_{Ld}{}^{*}, i_{Lq}{}^{*}]$.

C. Second-Order Large-Signal Model

As illustrated in Fig. 1(e), when the dynamics of the virtual inductors are ignored, (7) can be simplified as (10).

$$\begin{cases} R_v i_{Ld}{}^{*} - \omega_N L_v i_{Lq}{}^{*} = e_d{}^{*} - v_{od}{}^{\text{ctrl}} \\ \omega_N L_v i_{Ld}{}^{*} + R_v i_{Lq}{}^{*} = e_q{}^{*} - v_{oq}{}^{\text{ctrl}} \end{cases} \quad (10)$$

Thus, the 2nd-order large-signal model can be obtained by combining (1), (2), (5), (6), and (8)-(10), which is given by (11).

$$\begin{cases} \dot{\delta} = \Delta\omega + \omega_N - \omega_g \\ \Delta\dot{\omega} = -\omega_{LPF} \cdot \Delta\omega + \omega_{LPF} \cdot m_p \cdot [P^{*} - P(\delta)] \\ P(\delta) = \dfrac{3}{2} \cdot [i_{gd}{}^{g}(\delta) \cdot v_{od}{}^{g}(\delta) + i_{gq}{}^{g}(\delta) \cdot v_{oq}{}^{g}(\delta)] \end{cases} \quad (11)$$

where the voltage and current expressions are given by (12).

$$\begin{cases} i_{gd}{}^{g}(\delta) = [(R_v + R_g)(E^{*} \cdot \cos(\delta) - v_{gd}{}^{g}) \\ \qquad + (X_v + X_g)(E^{*} \cdot \sin(\delta) - v_{gq}{}^{g})] / \\ \qquad [(R_v + R_g)^2 + (X_v + X_g)^2] \\ i_{gq}{}^{g}(\delta) = [(-X_v - X_g)(E^{*} \cdot \cos(\delta) - v_{gd}{}^{g}) \\ \qquad + (R_v + R_g)(E^{*} \cdot \sin(\delta) - v_{gq}{}^{g})] / \\ \qquad [(R_v + R_g)^2 + (X_v + X_g)^2] \\ v_{od}{}^{g}(\delta) = R_g i_{gd}{}^{g}(\delta) - X_g i_{gq}{}^{g}(\delta) + v_{gd}{}^{g} \\ v_{oq}{}^{g}(\delta) = X_g i_{gd}{}^{g}(\delta) + R_g i_{gq}{}^{g}(\delta) + v_{gq}{}^{g} \end{cases} \quad (12)$$

Then, the large-signal stability analysis can be performed based on these reduced-order mathematical models.

IV. Large-Signal Stability Analysis

Due to the simplicity of the 2nd-order large-signal model, the 2nd-order large-signal model presented in (11) is preferable to use for large-signal stability analysis. The parameters of the study system are listed in Table I, and two study cases are selected for analysis.

A. Study Case 1: Impact of the depth of the grid voltage sag

As shown in Table I, the impact of the depth of the grid voltage sag is selected as the first study case. In Case 1, the initial active power is given to be 0.5 p.u. Then, the grid voltage V_g sags to 0.2, 0.3, and 0.4 p.u., respectively. The phase portrait of Study Case 1 is presented in Fig. 3. It shows that a deeper grid voltage sag is prone to cause transient instability.

TABLE I. Parameters of the Study Cases

General Parameters	Rated Power of inverter	30 kW
	Rated Voltage (line to line)	380 V (RMS)
	Nominal grid frequency	50 Hz
	Filter inductance, L_f	0.15 p.u.
	Filter capacitance, C_f	0.02 p.u.
	SCR and R_g/X_g	15 and 0.01
	P-ω droop coefficient, m_p	2.5% ω_N/P_N
	Virtual admittance, L_v and R_v	0.5 p.u. and 0.05 p.u.
Case 1	V_g sags to 0.2, 0.3, and 0.4 p.u. (P = 0.5 p.u.)	
Case 2	P is given 0.3, 0.5, and 0.7 p.u. (V_{g_fault} = 0.3 p.u.)	

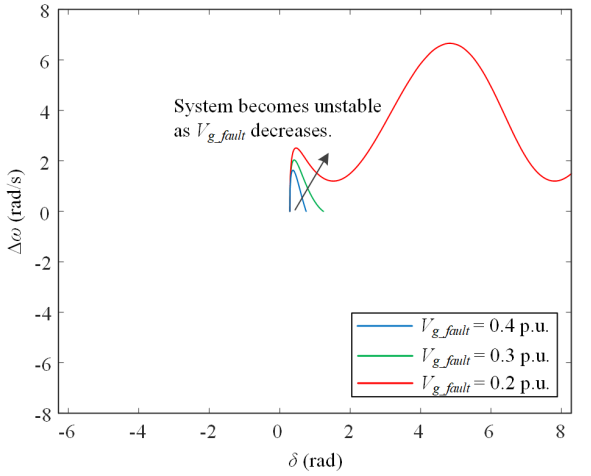

Fig. 3. Phase portrait of Study Case 1 (See Table I).

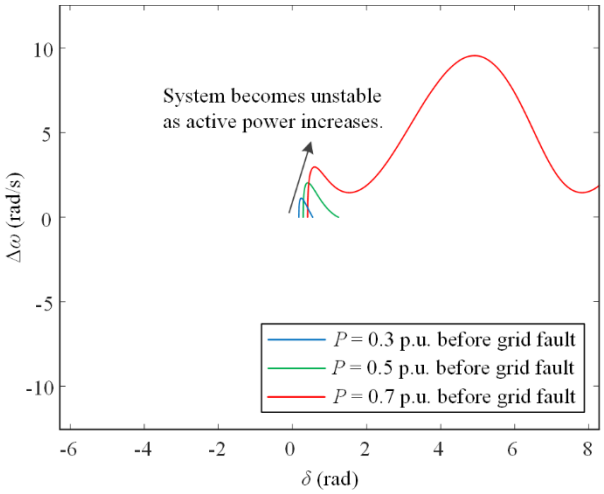

Fig. 4. Phase portrait of Study Case 2 (See Table I).

B. Study Case 2: Impact of the initial active power

As given in Table I, the impact of the initial active power is selected as the second study case. In Case 2, the initial active power is given to be 0.3, 0.5, and 0.7 p.u., respectively. Then, the grid voltage V_g sags to 0.3 p.u. The phase portrait of Study Case 2 is provided in Fig. 4. It shows that a higher active power of the inverter has a negative impact on the transient stability of the GFM inverter during grid faults.

C. Simulation Validation

To verify the correctness of the theoretical analysis, simulation studies of the GFM inverter are also carried out.

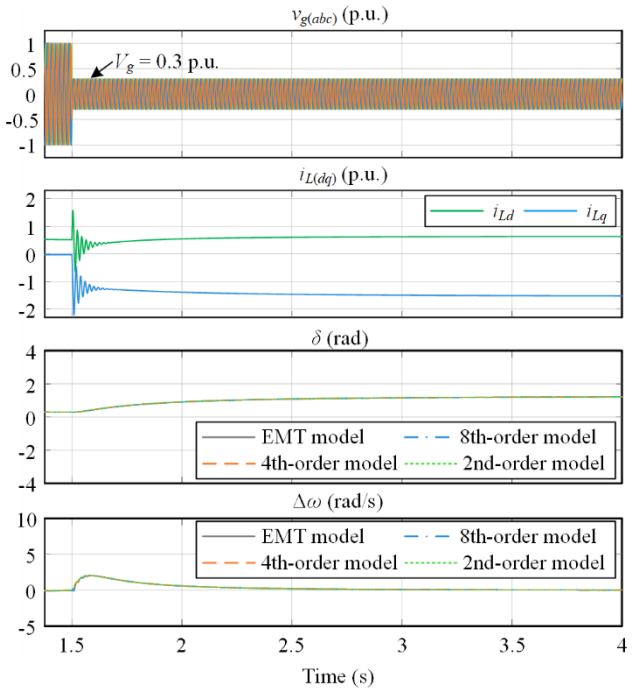

(a)

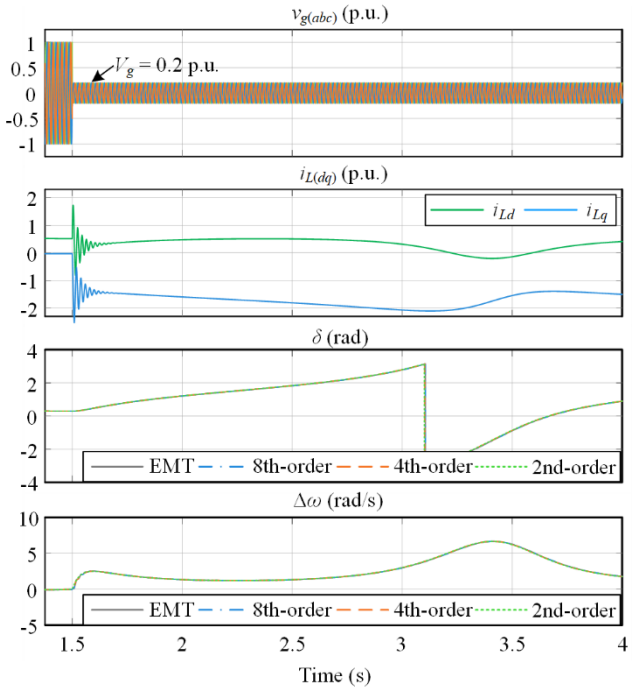

(b)

Fig. 5. Simulation results of Study Case 1. (a) V_g sags to 0.3 p.u., (b) V_g sags to 0.2 p.u.

The simulation results of Study Case 1 are given in Fig. 5. As presented in Fig. 5(a), when the grid voltage V_g sags to 0.3 p.u. under the initial condition of "P = 0.5 p.u.", the GFM inverter system is still stable. However, as shown in Fig. 5(b), when the grid voltage V_g sags to 0.2 p.u. under the same initial condition, the GFM inverter system becomes unstable. These simulation results agree with the theoretical analysis of Study Case 1 shown in Fig. 3.

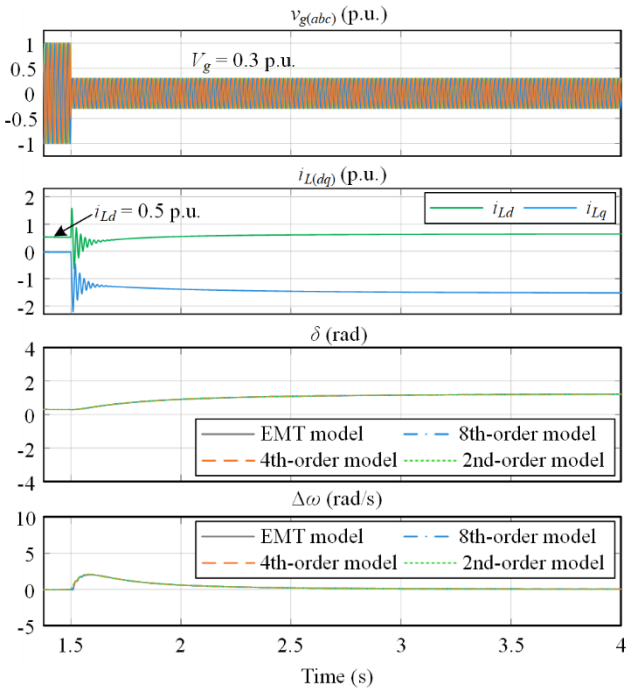

(a)

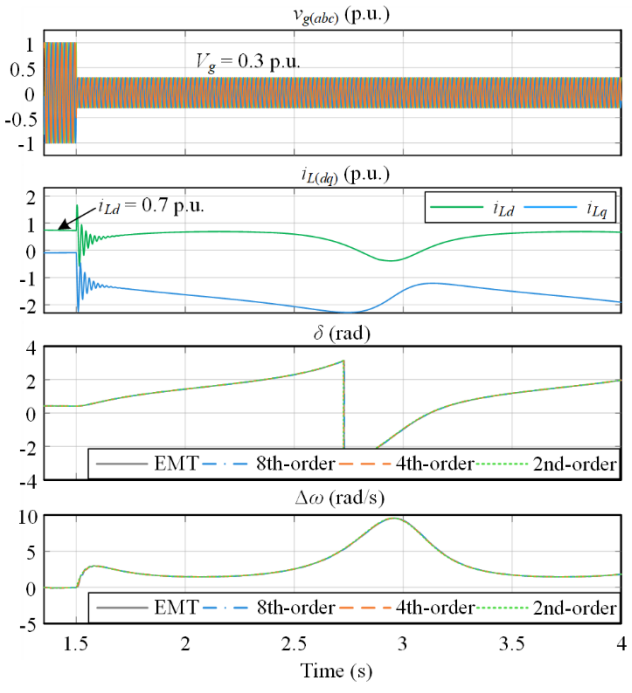

(b)

Fig. 6. Simulation results of Study Case 2. (a) Initial power is 0.5 p.u. before the grid voltage sag, (b) Initial power is 0.7 p.u. before the grid voltage sag.

In addition, the simulation results of Study Case 2 are provided in Fig. 6. As presented in Fig. 6(a), when the grid voltage V_g sags to 0.3 p.u. under the initial condition of "P = 0.5 p.u.", the GFM inverter is still stable. Nevertheless, as illustrated in Fig. 6(b), when the grid voltage V_g sags to 0.3 p.u. under the initial condition of "P = 0.7 p.u.", the GFM inverter system becomes unstable. These simulation results are consistent with the theoretical analysis of Study Case 2 shown in Fig. 4.

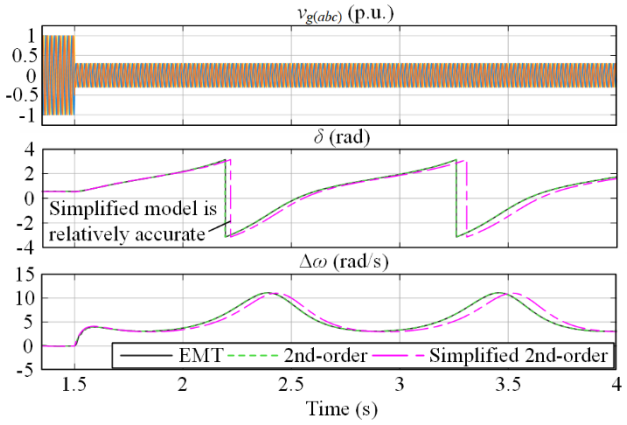

(a)

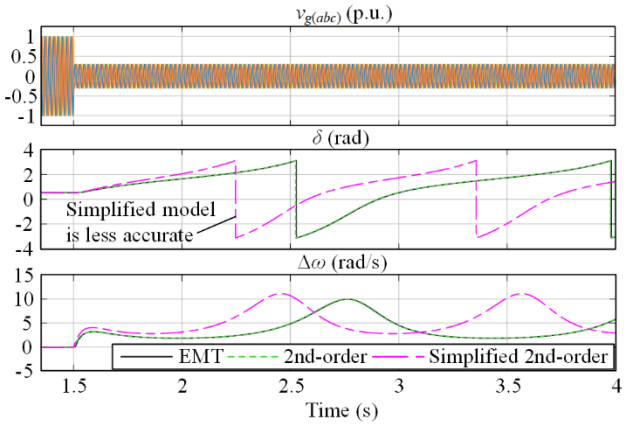

(b)

Fig. 7. Comparison of the proposed 2nd-order model in (11)&(12) and the simplified 2nd-order model in (11)&(13) by time-domain simulations. (a) In a smaller grid resistance case, (b) In a larger grid resistance case.

D. Further Discussion on Model Simplification

Although the 2nd-order large-signal model expressed by (11) and (12) shows accuracy and simplicity to some extent, (12) is still not straightforward. Considering that the grid resistance R_g and the virtual resistance R_v are relatively small, when assuming the resistances R_g and R_v equal to zero, (12) can be simplified further. In this case, the active power expression of the GFM inverter can be simplified as (13), which has the same form as the well-known power angle equation.

$$P(\delta) = \frac{3}{2} \cdot \frac{E^* \cdot V_g \cdot \sin(\delta)}{X_v + X_g}, \text{ if: } R_v = 0 \text{ and } R_g = 0 \qquad (13)$$

Simulation results of the proposed ordinary 2nd-order model in (11)&(12) and the simplified 2nd-order model in (11)&(13) are compared in Fig. 7. It shows that the simplified 2nd-order model becomes less accurate in a larger grid resistance case.

V. Conclusions

This paper provides several reduced-order large-signal models of the virtual admittance-based GFM inverter. By comparing these models, it is revealed that the 8th-order model, the 4th-order model, and the 2nd-order model have similar accuracy under grid voltage disturbances. It indicates that the dynamics of the current control loop, filter capacitors, grid inductors, and virtual inductors are negligible for large-signal stability analysis. In addition, the transient stability analysis results show that a higher active power before the grid faults and a deeper grid voltage sag during grid faults may lead to transient instability of the GFM inverter. Besides, when the grid resistance and virtual resistance are ignored, the proposed ordinary 2nd-order model can be derived as a simplified 2nd-order model. The simplified 2nd-order model has higher accuracy in a smaller grid resistance case, while it becomes less accurate in a larger grid resistance case, which is a potential limitation. At last, it is worth mentioning that the impact of the current limitations on the GFM inverter is not considered in this paper, and this will be studied further in the future.

References

[1] K. Strunz, K. Almunem, C. Wulkow, M. Kuschke, M. Valescudero, and X. Guillaud, "Enabling 100% renewable power systems through power electronic grid-forming converter and control: system integration for security, stability, and application to Europe," *Proc. IEEE*, vol. 111, no. 7, pp. 891–915, Jul. 2023.

[2] L. Huang, C. Wu, D. Zhou, L. Chen, D. Pagnani, and F. Blaabjerg, "Challenges and potential solutions of grid-forming converters applied to wind power generation system—An overview," *Front. Energy Res.*, vol. 11, p. 1040781, Jan. 2023.

[3] S. D'Arco and J. A. Suul, "Virtual synchronous machines - Classification of implementations and analysis of equivalence to droop controllers for microgrids," in *2013 IEEE Grenoble Conference*, Grenoble, France, 2013, pp. 1–7.

[4] P. Rodriguez, I. Candela, and A. Luna, "Control of PV generation systems using the synchronous power controller," in *2013 IEEE Energy Conversion Congress and Exposition*, Denver, CO, USA, 2013, pp. 993–998.

[5] A. Tayyebi, D. Gross, A. Anta, F. Kupzog, and F. Dorfler, "Frequency stability of synchronous machines and grid-forming power converters," *IEEE J. Emerg. Sel. Top. Power Electron.*, vol. 8, no. 2, pp. 1004–1018, Jun. 2020.

[6] "Grid forming capability of power park modules," European Network of Transmission System Operators for Electricity, Tech. Rep., 2024.

[7] N. Hatziargyriou *et al.*, "Definition and classification of power system stability – revisited & extended," *IEEE Trans. Power Syst.*, vol. 36, no. 4, pp. 3271–3281, Jul. 2021.

[8] S. Ghimire *et al.*, "Functional specifications and testing requirements for grid-forming offshore wind power plants," *Wind Energy Sci.*, vol. 10, no. 1, pp. 1–15, Jan. 2025.

[9] N. Klaes and J. Fortmann, "Immunity of grid-forming control without energy storage to transient changes of grid frequency and phase," *IEEE Open J. Ind. Electron. Soc.*, 2025 (Early Access).

[10] M. G. Taul, X. Wang, P. Davari, and F. Blaabjerg, "An overview of assessment methods for synchronization stability of grid-connected converters under severe symmetrical grid faults," *IEEE Trans. Power Electron.*, vol. 34, no. 10, pp. 9655–9670, Oct. 2019.

[11] X. Xiong, C. Wu, and F. Blaabjerg, "Effects of virtual resistance on transient stability of virtual synchronous generators under grid voltage sag," *IEEE Trans. Ind. Electron.*, vol. 69, no. 5, pp. 4754–4764, May 2022.

[12] X. Fu *et al.*, "Large-signal stability of grid-forming and grid-following controls in voltage source converter: a comparative study," *IEEE Trans. Power Electron.*, vol. 36, no. 7, pp. 7832–7840, Jul. 2021.

[13] X. He, S. Pan, and H. Geng, "Transient stability of hybrid power systems dominated by different types of grid-forming devices," *IEEE Trans. Energy Convers.*, vol. 37, no. 2, pp. 868–879, Jun. 2022.

[14] A. Hadjileonidas, Y. Li, and T. C. Green, "Comparative analysis of transient stability of grid-forming and grid-following inverters," in *2022 IEEE International Power Electronics and Application Conference and Exposition (PEAC)*, Guangzhou, China, 2022, pp. 296–301.